International Journal of Science & Technology (PRAGYANAM)
Volume 1 • Issue 1 • January–December 2025
ISSN:

Organic Solar Cell Based with Inorganic Transport Layers: Performance Analysis and Optimisation

Iram Masood[1], Mukesh Pratap Singh[2] & Mohd Amir[3]

ABSTRACT

The use of transport layers (with high carrier mobilities) in organic solar cells result in high charge carrier extraction efficiency. In this work, inorganic materials, i.e. ZnO and NiO are utalised as electron and hole transport layers. The thicknesses of each layer in the device structure ITO (anode)/NiO/P3HT:PCBM/ZnO/Al (cathode) of an OSC are optimised. The effect of potential loss mechanisms on the device performance is also studied in this work. Subsequently, the effect of temperature variation on the performance of the device is studied. It is observed as the temperature increases from 250 to 400 K, the short-circuit current density (J_{SC}) increases, while the fill-factor (FF) and open circuit voltage (V_{OC}) of the device shows an inverse dependency on temperature. We have used an open-source computer-based program OghmaNano to perform the calculations in this work.

Keywords: Organic Solar Cells (OSCs), Optimisation, Recombination, Temperature, OghmaNano Software

INTRODUCTION

In present scenario, it is a need of the hour to have a reliable energy harvesting source that is cost effective and sustainable [1]. The most prominent reliable energy source is solar energy, and it may be harvested by the means of solar cells. These cells shows high potential to meet our current and future energy requirement. The silicon (Si) based solar cells dominates the today's market of solar cells mainly due to their excellent stability and high power conversion efficiency (*PCE*) [2,3]. The manufacturing of these cells include sophisticated machinery leading to increased cost of power per unit. For the past few years, different types of solar cells have been introduced to replace Si based solar cells, continuous research and efforts are being made to bring their *PCE* as high as possible. Recently, the thin-film solar cell technology has caught the attention of scientific fraternity to contribute towards its development and make use of the same to serve the community [4]. The semiconducting polymer and small molecule based organic solar cell (OSCs) technology is suitable to the required demand as it supports ease of fabrication, i.e. cost-effective roll to roll processing and flexibility [5]. However, unlike Si based solar cells, the OSCs have limitation of small *PCEs* and their poor lifetime has triggered the interest to overcome OSCs limitations [2]. Among, all the available varieties of OSCs, the bulk heterojunction (BHJ) OSCs have the advantage of using blend of Donor (D) and Acceptor (A) materials with the selective properties which can possibly be produced by inexpensive fabrication methods [6]. The interconnecting mixture of donor material, i.e. P3HT and acceptor material like PCBM, is used as photon absorbing active material deposited between anode and cathode in BHJ OSCs [6,7]. To forbid the direct contact of active material with the electrodes, and to accelerate the selective charge carrier collection at the reference electrode, the hole and electron transport layers (HTL & ETL) are deposited on anode (below active layer) and cathode (adjacent to active layer), respectively. The thickness optimisation of these ETL and HTL layers promote light absorption within the active layer [7]. A conducting polymer, PEDOT:PSS is the most dominating conducting polymer in the field of OSCs, PEDOT:PSS is recognized for its good conductivity

[1] Department of Applied Sciences & Humanities, Jamia Millia Islamia, New Delhi, India. E-mail: iram188891@st.jmi.ac.in
[2] Department of Applied Sciences & Humanities, Jamia Millia Islamia, New Delhi, India. E-mail: mpsingh@jmi.ac.in
[3] Department of Applied Sciences & Humanities, Jamia Millia Islamia, New Delhi, India. E-mail: mohd169066@st.jmi.ac.in

and transparency (particularly in the visible wavelength range), temperature stability and easy solution-based fabrication-process, but due to the acidic tendency of PEDOT:PSS, the stability of device is affected [8,9].

The metal oxides such as tungsten trioxide (WO_3), zinc oxide (ZnO), nickel oxide (NiO), molybdenum trioxide (MoO_3), and titanium dioxide (TiO_2), show better stability in ambient and may be used as charge carrier transport layers based on their band energies, in OSCs device structure [10-13]. We have selected a positive type hole accepting metal oxide, i.e. NiO as HTL which has broad energy gap, high electron affinity and good conductivity, while ZnO is selected as ETL due to its wide bandgap (3.3 eV), ambient stability, low absorption, transparency in the visible range and good electron mobility [12-16]. In present study the thicknesses of each layer in the stack of an OSC is optimised to enhance the *PCE* of the device. The effect of potential loss mechanisms such as geminate and non-geminate recombination on the performance of the OSC is studied. Furthermore, the device performance is evaluated by varying the temperature and its effect on the OSC parameters such as power conversion efficiency (*PCE*), fill factor (*FF*), short circuit current density (J_{SC}), and open circuit voltage (V_{OC}) is detailed insight.

DEVICE SIMULATION USING OGHMANANO SOFTWARE

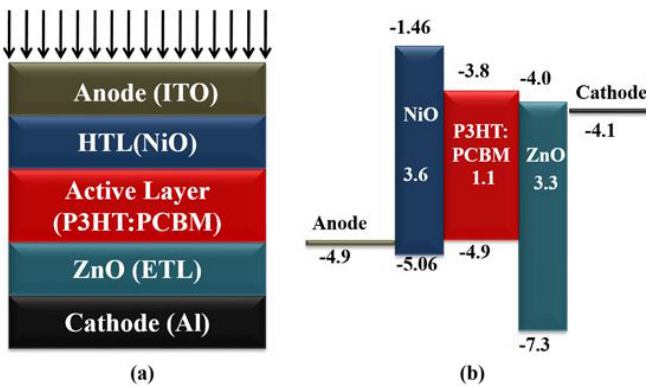

Fig. 1. (a) The schematic of the designed organic solar cell, (b) Energy band diagram of the materials

The schematic of the simulated device and the energy states diagram are presented in the Fig. 1(a) and Fig. 1(b), respectively. We have used an open source, opto-electronic device simulation software OghmaNano supports drift and diffusion transport model for charge carriers, evaluate charge carrier recombination and trapping [17]. The OghmaNano software offers a material database and is compatible to add new materials with different properties to it. The parameters of the material can be controlled within the program, and maximum of 10 layers can be simulated at once.

The program examine the electrical behaviour of the simulated device by solving equations (1) numerically to obtain the potential distribution (φ) with the device [17-18].

$$\varepsilon_0 \varepsilon_r \nabla\varphi = q\,(n_f - p_f + n_t - p_t) \qquad ...(1)$$

Where q is the electron charge, ε_0 is the free space permittivity while the permittivity of the material used as active layer is ε_r. The quantities n_f / p_f represents the free carrier concentration of electron/hole, while the trapped concentration is denoted with n_t / p_t for electron/hole [17]. The continuity equations, described by the equations (2) and (3) are solved to obtain the concentrations of free carriers (i.e. electrons and holes)

$$\nabla J_n = q\,(R_e - G) \qquad ...(2)$$

$$\nabla J_p = q\,(R_h - G) \qquad ...(3)$$

in terms of net recombination ($R_{e/h}$) and free electrons/holes generation rates (G). Finally, to obtain the total electron current (J_n) and hole current (J_p), drift-diffusion equation, i.e. equations (4) and (5) are solved.

$$J_n = q[n_f \mu_e \cdot(\partial E_{LUMO}/\partial x) + (\partial n_f/\partial x) D_n] \qquad ...(4)$$

$$J_p = q\,[p_f \mu_h\,(\partial E_{HOMO}/\partial x) + (\partial p_f/\partial x)\,D_p] \qquad ...(5)$$

Here $D_n(D_p)$ are diffusion coefficients of electrons (holes), μ_e/μ_h is the mobility of electrons/holes. The Shockley-Read-Hall recombination model is followed for charge carrier trapping and recombination [17,18]. The required density of states parameters in the program are listed in Table 1. The Fig. 2 depicts simulated device structure in OghmaNano simulation window.

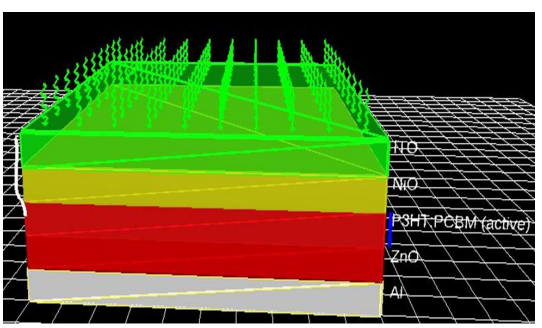

Fig. 2. The simulated device snap-shot of OghmaNano simulation window

Table 1. The density of states parameters

Simulation Parameters for Active layer		
Parameters	*Values*	*Units*
Trap density (electron)	3.8×10^{26}	(m^{-3}/eV)
Hole trap density	1.45×10^{25}	(m^{-3}/eV)
Mobility (electron)	2.48×10^{-7}	(m^2/V/s)
Mobility (hole)	2.48×10^{-7}	(m^2/V/s)
Tail slope for electron	0.04	(eV)
Tail slope for hole	0.06	(eV)
Free electron density of states	1.28×10^{27}	(/m^3)
Free hole density of states	2.86×10^{25}	(/m^3)
Material relative permittivity	3.8	–
Total traps number	20	(bands)
Electron affinity	3.8	(eV)
Energy gap	1.1	(eV)
Trapped electron to free electron	2.5×10^{-20}	(/m^2)
Trapped hole to free hole	4.86×10^{-22}	(/m^3)
Trapped electron to free hole	1.32×10^{-22}	(/m^2)
Trapped hole to free electron	4.67×10^{-26}	(/m^2)

RESULTS AND DISCUSSION

The investigation of active layer (P3HT:PCBM), transport layers and electrodes thicknesses is of immense importance for electron/hole generation, transportation and collection within the OSC device and its effect on parameters of OSC. We made a variation from 60 to 300 nm in the active layer thickness in order to find its optimum value. The obtained current voltage (*J-V*) characteristics and the corresponding OSC parameters at different values of active layer thicknesses are plotted in Fig. 3 and 4, respectively. The open circuit voltage (V_{OC}) is energy levels (active material) dependent, in Fig. 4. The maximum value of V_{OC} is obtained as 0.59 V at 170 nm of the active layer thickness. The current density (J_{SC}) is mainly depends on the exciton (loosely bounded electron hole pair) generation upon the absorption of incident light in active layer.

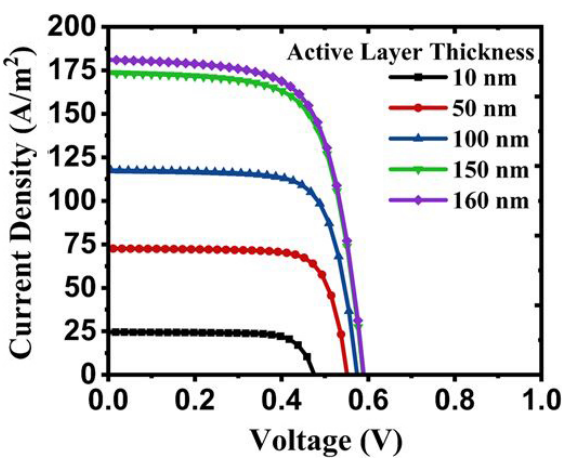

Fig. 3. Effect of active layer thickness on *J-V* characteristics

It has observed in the results, a thin active layer leads to less photon absorption resulting in lower J_{SC}. The path length travelled by the free charge carriers increases as the thickness of the active layer increases which results in lower charge carrier collection efficiency and hence the current density of the device reduces. The maximum value of J_{SC} is obtained as 187.10 A/m^2 at the thickness of 170 nm. The increase in the active layer thickness also leads to high series resistance resulting in the degradation of fill factor (*FF*), shown in Fig. 3. Consequently, thickness of active layer is optimised as 170 nm, resulting in maximum *PCE* of 7.28%. The value of *FF* is obtained as 65.86% at the optimised thickness of active layer.

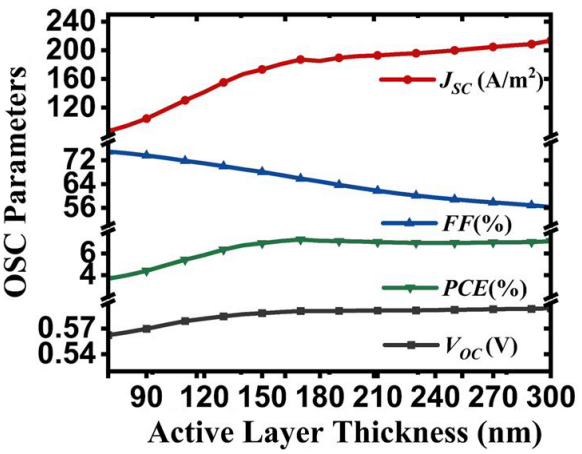

Fig. 4. Effect of thickness variation of active layer on OSC parameters

The transport layers (ETL and HTL) thicknesses are varied from 1 to 100 nm. The OSC parameters as a function of thickness variation of hole selective layer or HTL (NiO) is depicted in Fig. 5 and Fig. 6 shows the *J-V* curves at different values of the HTL thickness. The J_{SC} increases up to 5 nm of HTL thickness due to reduced reflection. The light transmittance is limited by the further increase in HTL thickness and series resistance increase with the increase in HTL thickness which reduces J_{SC} and degrades the *FF*. So, the optimised thickness of HTL is considered as 5 nm, leading to a *PCE* of 7.35%. The value of V_{oc} is obtained as 0.59 V while the values of J_{SC} and *FF* are attained as 188.76 A/m^2 and 65.88%, respectively with the HTL thickness of 5 nm.

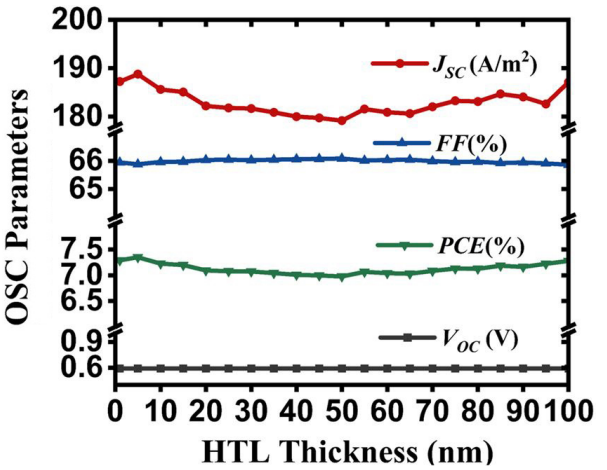

Fig. 5. Effect of thickness variation of HTL on OSC parameters

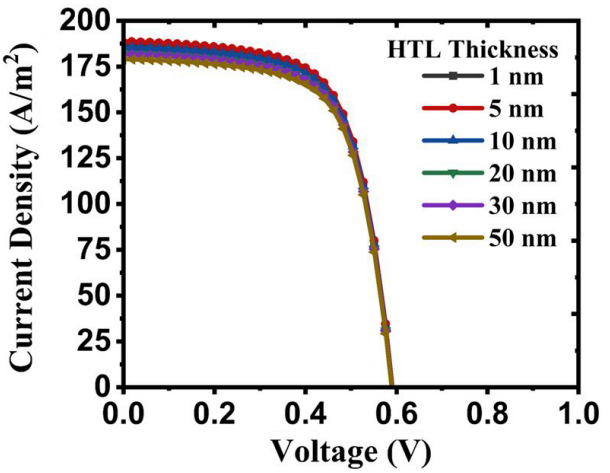

Fig. 6. Effect of HTL thickness on *J-V* characteristics

The Fig. 7 shows the effect of ETL (ZnO) thickness variation upon the *J-V* characteristics of the device. The ETL also known as electron selective layer, act as a barrier to stop the direct contact of active layer and cathode. The effect of ETL (ZnO) thickness has also been examined on the parameters of the OSC and plotted in Fig. 8. It is observed as the thickness of ETL increases no significant change occurs in the V_{OC} and *FF*. However, the J_{SC} increases up to 50 nm of ETL thickness, leading to increase in the *PCE* as can be observed in the Fig. 8. The advancement in J_{SC} and *PCE* on an increase in ELT thickness up to 50 nm attributed to the decrease reflection loses of the device. Whereas the reflection increases significantly beyond the 50 nm of ETL lowering the fraction of absorbed light within the active layer, causing a decrease in J_{SC} as well as in *PCE*. Moreover the increase in ETL thickness beyond 50 nm significantly increases the recombination of free charge carriers adding further decay to J_{SC}. Hence the thickness of ETL is optimised as 50 nm resulting in a maximum *PCE* of 7.30%.

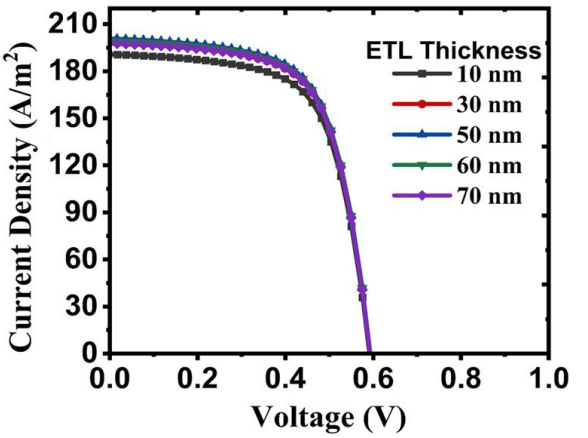

Fig. 7. Effect of ETL thickness on *J-V* characteristics.

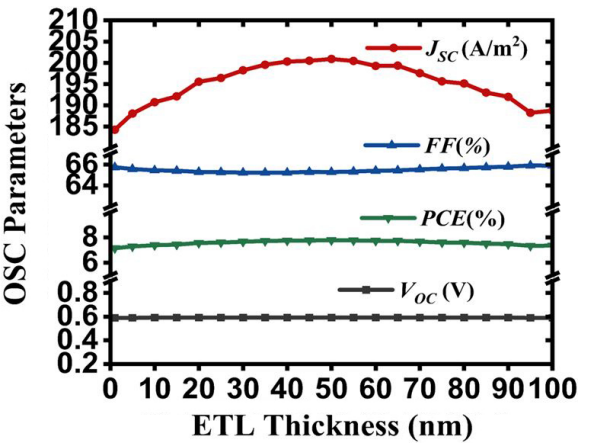

Fig. 8. Effect of ETL thickness on OSC parameters

In order to examine the effect of electrodes (anode and cathode) thicknesses on the device, their thicknesses are changed from 1 nm to 100 nm. The OSC parameters are shown in Fig. 9 for the change in anode thickness, and impact of anode thickness on *J-V* characteristics is depicted in the Fig. 10.

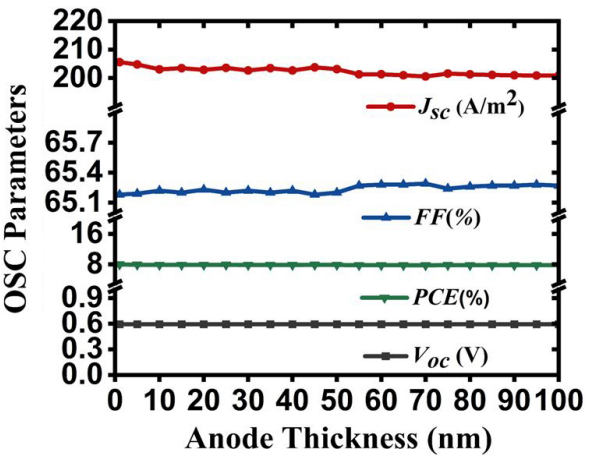

Fig. 9. Effect of anode thickness on OSC parameters

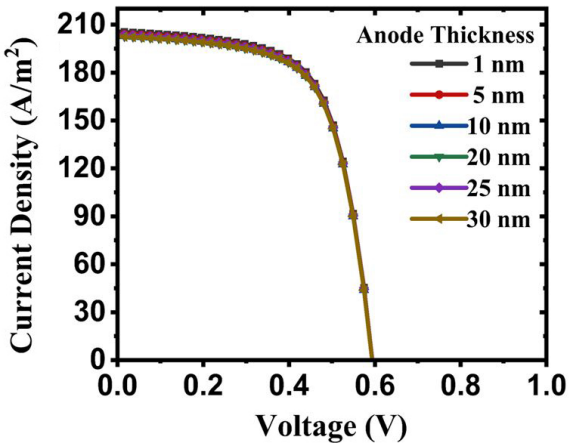

Fig. 10. Effect of anode thickness on *J-V* characteristics

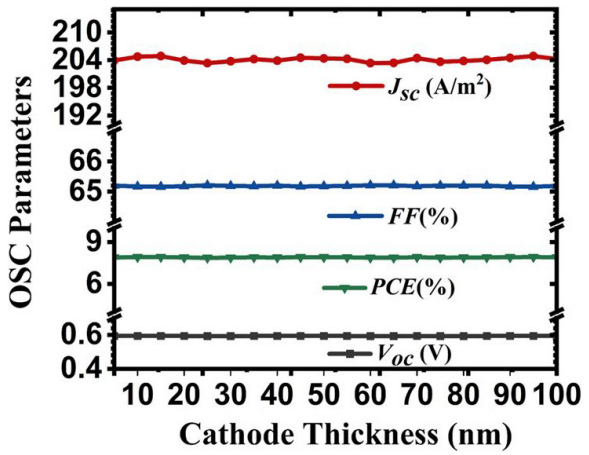

Fig. 11. The effect of cathode thickness on OSC parameters

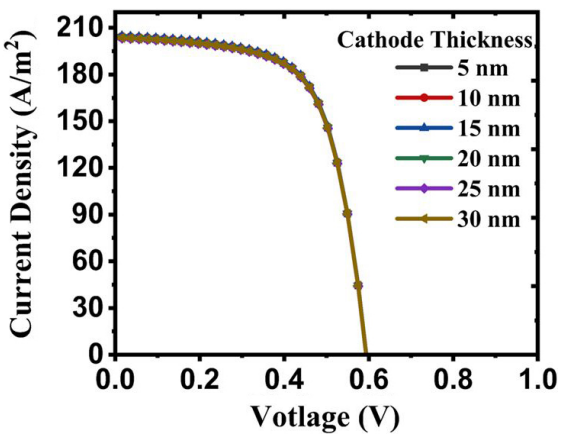

Fig. 12. Effect of cathode thickness on *J-V* characteristics

The effect of cathode thickness variation on *J-V* characteristics are represented in Fig. 11 and the corresponding OSC parameters are plotted in Fig. 12.

The anode (ITO) is the top most layer in the device structure hence it must be thin enough to enhance light transmission towards the active layer. After examining OSC parameters as shown in the Fig. 9 the optimised value of its thickness is obtained as 5 nm, resulting a *PCE* of 7.91%. The cathode (Al) reflects back the portion of light to the active layer, this slightly enhances J_{SC} initially. The optimal thickness of cathode is found to be 15 nm. After the optimisation cathode thickness the values of *Voc*, J_{SC} and *FF* are as 0.59 V, 204.86 A/m^2 and 65.16% respectively, with 7.93% of *PCE*.

Now for the device with the optimised layer thicknesses, we investigated the effect of recombination (geminate & non-geminate) on the device performance. The impact of geminate recombination on OSC parameters are shown in Fig. 13 and *J-V* characteristics are represented in the Fig. 14.

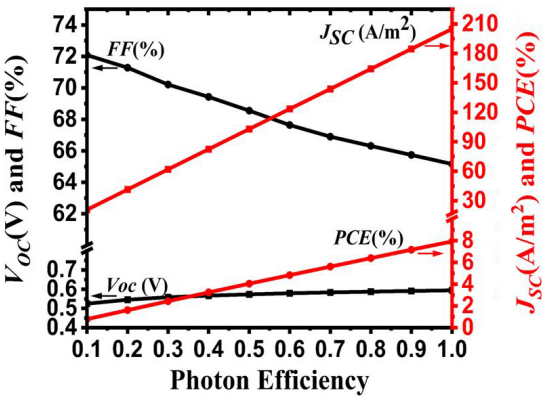

Fig. 13. Effect of geminate recombination on OSC parameters

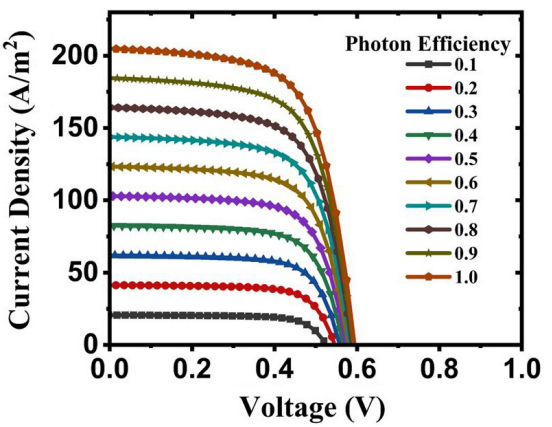

Fig. 14. Effect of geminate recombination on *J-V* characteristics

The geminate recombination takes place before the charge separation for the same photo generated exciton. If the dissociation of bound electron-hole could not proceed, they will relax into ground state, recombining together. The separation of bounded excitons is measured in terms of photon efficiency, where 100% (or 1) photon efficiency means that each photo generated exciton successfully separate into the free electron hole pairs. The variation in OSC

parameters due to geminate recombination at low and higher photon efficiencies are plotted in Fig. 13. The results show that at 40% photon efficiency, the *PCE* is attained as 2.42%. which implies that 60% of photon generated excitons are not being separated at charge transfer state (CTS), enabling geminate recombination. Whereas at higher photon efficiencies, J_{SC} and *PCE* becomes high due to lower geminate recombination, as more excitons dissociate at the CTS. At 90% photon efficiency, *PCE* is obtained as 7.16%.

Once all the photo generated excitons are separated into free electron hole pairs there is a high chance that these moving (freely) pairs may recombine together which is known as the non-geminate recombination of free carriers. To examine the effect of non-geminate recombination on the performance of the device we have varied the recombination coefficient (*R*) form 1×10^{-10} to 1×10^{-25} m^3/s and the obtained OSC parameters as represented in the Fig. 15 while the correspondingly obtained *J-V* characteristics are shown in Fig. 16.

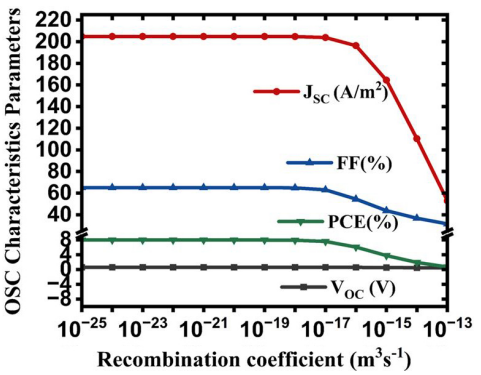

Fig. 15. Effect of non-geminate recombination on OSC parameters

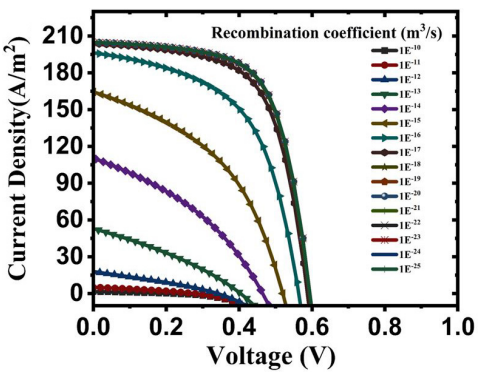

Fig. 16. Effect of non-geminate recombination on *J-V* characteristics.

It has observed with the increase in *R* the OSC parameters remains unaffected up to 1×10^{-20} m^3/s of *R*. The further increase in *R* leads to more enhanced non-geminate recombination, resulting the degradation in all the OSC parameters. The best value of *PCE* (7.93%) is achieved with the *R* values of 1×10^{-20} m^3/s.

To examine the effect of temperature (*T*), it is varied from 250K to 400 K and the resulted parameters of the OSC are plotted in the Fig. 17. The results show that the parameters of OSC specially J_{SC}, *FF* and *PCE* are severely affected as the temperature increases. It can also be seen in the Fig. 17 the change in temperature from 250K to 400K decreases V_{OC} drastically from 0.59 to 0.44 Volts. The values of fill factor degrades from 62% to 59% and *PCE* declines and 7.93% to 5.23%. The increment in short circuit current density (J_{SC}), from 204.33 to 206.03 A/m^2 with the increase in temperature from 250K to 400K is mainly attributed to the enhanced thermally generated carrier concertation. Moreover above the 400K, all the OSC parameters severely degrades.

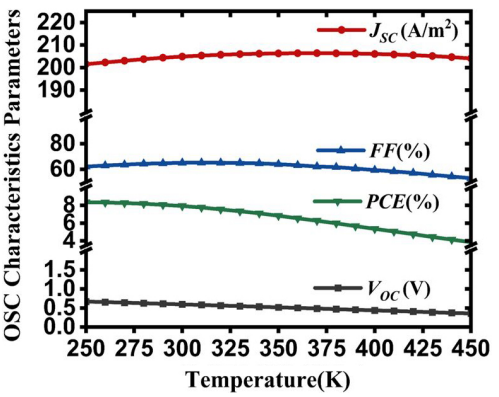

Fig. 17. Effect of temperature on OSC parameters

Since the increment rate of J_{SC} is minor than the degradation rate of V_{OC} and hence the *PCE* and the fill factor are reduced. The good performance of device is found to be at 300K as higher temperature leads to poor device performance. The optimum values of OSC parameters at the optimised values of the corresponding layer thicknesses are listed in the Table 2 at 300K.

Table 2. The OSC parameters obtained with the optimised layer thicknesses at 300K

Electrical parameter values at optimised thicknesses					
Layer	*Thickness (nm)*	V_{OC} *(V)*	J_{SC} *(A/m²)*	*FF (%)*	*PCE (%)*
Active	170	0.591	187.104	64.85	7.28
HTL	5	0.591	188.76	65.88	7.35
ETL	50	0.593	200.91	65.27	7.78
Anode	5	0.594	118.75	65.19	7.91
Cathode	15	0.594	204.86	65.16	7.93

CONCLUSION

The organic solar cell with the active layer P3HT: PCBM has been analysed by a computer based program, i.e. OghmaNano. After closely monitoring the variation in OSC parameters as a function of each layer thicknesses the thicknesses of all the layers within the structure of the designed device is been optimised. The resulted optimised values of active layer, ETL, HTL, cathode and anode are found to be 170, 50, 5, 15, and 5 nm, respectively. The optimisation has resulted a maximum *PCE* of 7.93%. The device performance is also been analysed for the effect of recombination (i.e., geminate & non-geminate). The best *PCE* of the device is found at 1×10^{-20} m^3/s value of *R*. Moreover, the parameters of the OSC are studied at different values of the temperature. It is concluded that the *PCE* degrades with rise in temperature. The *PCE* of 7.93% is obtained at 300 K. The result obtained in our work is compared with the existing work in literature and listed in Table 3.

Table 3. The comparison of our work with results obtained in literature

Structure of Device	V_{OC} *(V)*	J_{SC} *(A/m²)*	*FF (%)*	*PCE (%)*	*Ref.*
ITO/NiO/ P3HT:PCBM/ZnO/Al	0.59	204.8	65.16	7.93	This work
ITO/PEDOT:PSS/ P3HT:PCBM/Ca/Al	0.62	98.0	59.51	3.62	[19]
ITO/PEDOT:PSS/ P3HT:PCBM/TiO_2/Al	0.61	129.5	67.91	5.35	[6]
ITO/PEDOT:PSS/ P3HT:PCBM/Al	0.52	74.7	46.0	1.78	[21]
ITO/ZnO/P3HT: PCBM/MoO_3/Ag	0.60	131.9	65.0	5.23	[22]

ACKNOWLEDGMENT

The authors are highly thankful to the Prof. Mackenzie for giving us free access to the program (OghmaNano).

REFERENCES

[1] Medford, A.J., Lilliedal, M.R., Jørgensen, M., Aarø, D., Pakalski, H., Fyenbo, J., & Krebs, F.C. (2010). Grid-connected polymer solar panels: Initial considerations of cost, lifetime, and practicality. *Optics Express*, *18*(103), A272-A285.

[2] Chen, L.X. (2019). Organic solar cells: Recent progress and challenges. *ACS Energy Letters*, *4*(10), 2537-2539.

[3] Chopra, K.L., Paulson, P.D., & Dutta, V. (2004). Thin-film solar cells: An overview. *Progress in Photovoltaics: Research and applications*, *12*(2-3), 69-92.

[4] Krebs, F.C., & Jørgensen, M. (2013). Polymer and organic solar cells viewed as thin film technologies: What it will take for them to become a success outside academia. *Solar energy materials and solar cells*, *119*, 73-76.

[5] Kaltenbrunner, M., White, M.S., Głowacki, E.D., Sekitani, T., Someya, T., Sariciftci, N.S., & Bauer, S. (2012). Ultrathin and lightweight organic solar cells with high flexibility. *Nature communications*, *3*(1), 1-7.

[6] Abdallaoui, M., Sengouga, N., Chala, A., Meftah, A.F., & Meftah, A.M. (2020). Comparative study of conventional and inverted P3HT: PCBM organic solar cell. *Optical Materials*, *105*, 109916.

[7] Berger, P.R., & Kim, M. (2018). Polymer solar cells: P3HT: PCBM and beyond. *Journal of Renewable and Sustainable Energy*, *10*(1), 013508.

[8] Zhang, X., Yang, W., Zhang, H., Xie, M., & Duan, X. (2021). PEDOT:PSS: From conductive polymers to sensors. *Nanotechnology and Precision Engineering*, *4*(4), 045004.

[9] Tseng, Y.T., Lin, Y.C., Shih, C.C., Hsieh, H.C., Lee, W.Y., Chiu, Y.C., & Chen, W.C. (2020). Morphology and properties of PEDOT: PSS/soft polymer blends through hydrogen bonding interaction and their pressure sensor application. *Journal of Materials Chemistry C*, *8*(18), 6013-6024.

[10] Yang, T., Wang, M., Cao, Y., Huang, F., Huang, L., Peng, J., & Cao, Y. (2012). Polymer solar cells with a low-temperature-annealed sol-gel-derived MoOx film as a hole extraction layer. *Advanced Energy Materials*, 2(5), 523-527.

[11] Tan, Z. A., Li, L., Cui, C., Ding, Y., Xu, Q., Li, S., ... & Li, Y. (2012). Solution-processed tungsten oxide as an effective anode buffer layer for high-performance polymer solar cells. *The Journal of Physical Chemistry C*, *116*(35), 18626-18632.

[12] Tiwari, D.C., Dwivedi, S.K., Dipak, P., Chandel, T., & Sharma, R. (2017, May). Sol-gel derived ZnO as an electron transport layer (ETL) for inverted organic solar cells. In *AIP Conference Proceedings* (Vol. 1832, No. 1, p. 060024). AIP Publishing LLC.

[13] Irwin, M. D., Buchholz, D. B., Hains, A. W., Chang, R. P., & Marks, T. J. (2008). p-Type semiconducting nickel oxide as an efficiency-enhancing anode interfacial layer in polymer bulk-heterojunction solar cells. *Proceedings of the National Academy of Sciences*, *105*(8), 2783-2787.

[14] Mahmud, M.A., Elumalai, N.K., Upama, M. B., Wang, D., Chan, K.H., Wright, M., ... & Uddin, A. (2017). Low temperature processed ZnO thin film as electron

transport layer for efficient perovskite solar cells. *Solar Energy Materials and Solar Cells*, *159*, 251-264.

[15] Sun, N., Fang, G., Qin, P., Zheng, Q., Wang, M., Fan, X., ... & Ye, J. (2010). Efficient flexible organic solar cells with room temperature sputtered and highly conductive NiO as hole-transporting layer. *Journal of Physics D: Applied Physics*, *43*(44), 445101.

[16] Kumar, D., Singh, M.K., & Mehata, M.S. (2022). Exploration of grown cobalt-doped zinc oxide nanoparticles and photodegradation of industrial dye. *Materials Research Bulletin*, *150*, 111795.

[17] MacKenzie, R.C. (2022). Gpvdm user manual v7. 88.

[18] MacKenzie, R.C., Shuttle, C.G., Chabinyc, M.L., & Nelson, J. (2012). Extracting microscopic device parameters from transient photocurrent measurements of P3HT: PCBM solar cells. *Advanced Energy Materials*, *2*(6), 662-669.

[19] Brioua, F., Remram, M., Nechache, R., & Bourouina, H. (2017). Electrical and optical modeling of poly (3-hexylthiophene):[6, 6]-phenyl-C61 butyric acid methyl ester P3HT–PCBM bulk heterojunction solar cells. *Applied Physics A*, *123*, 1-10.

[20] Korte, D., Pavlica, E., Klančar, D., Bratina, G., Pawlak, M., Gondek, E.,& Derkowska-Zielinska, B. (2023). Influence of P3HT: PCBM Ratio on Thermal and Transport Properties of Bulk Heterojunction Solar Cells. *Materials*, *16*(2), 617.

[21] Husen, M.J., Aga, F.G., & Dibaba, S.T. (2023). Theoretical Performance Analysis of Inverted P3HT: PCBM Based Bulk Hetero-Junction Organic Solar Cells through Simulation. *Advances in Materials Science and Engineering*, *2023*.